CrossMark

J. Fluid Mech. (2016), *vol.* 789, *pp.* 500–513. © Cambridge University Press 2016
doi:10.1017/jfm.2015.747

Strong-field spherical dynamos

Emmanuel Dormy†

MAG (CNRS/IPGP/ENS), Ecole Normale Supérieure, 24 Rue Lhomond, 75005 Paris, France

(Received 7 December 2014; revised 31 October 2015; accepted 15 December 2015;
first published online 22 January 2016)

Numerical models of the geodynamo are usually classified into two categories: dipolar modes, observed when the inertial term is small enough; and multipolar fluctuating dynamos, for stronger forcing. We show that a third dynamo branch corresponding to a dominant force balance between the Coriolis force and the Lorentz force can be produced numerically. This force balance is usually referred to as the strong-field limit. This solution coexists with the often described viscous branch. Direct numerical simulations exhibit a transition from a weak-field dynamo branch, in which viscous effects set the dominant length scale, and the strong-field branch, in which viscous and inertial effects are largely negligible. These results indicate that a distinguished limit needs to be sought to produce numerical models relevant to the geodynamo and that the usual approach of minimising the magnetic Prandtl number (ratio of the fluid kinematic viscosity to its magnetic diffusivity) at a given Ekman number is misleading.

Key words: geodynamo, geophysical and geological flows, magnetohydrodynamics

1. Introduction

The origin of the Earth's magnetic field is a challenging problem. It is now widely accepted that this magnetic field is generated by an internal self-excited dynamo action in the conducting liquid core of the Earth – see Moffatt (1978) and Dormy & Soward (2007) for an introduction. Thermal energy is converted to kinetic energy via convective motions, which in turn are able to amplify electrical currents, and part of the kinetic energy can thus be converted to magnetic energy. The amplification of electrical currents in the conducting fluid is then saturated by the back-reaction of the Lorentz force on the flow. The nature of the transition from a purely hydrodynamic (non-magnetic) solution to the dynamo solution as well as the saturation mechanisms remain largely open questions.

The geodynamo problem involves the resolution of a set of fully nonlinear coupled equations describing magnetohydrodynamics (MHD) in a rotating reference frame. In the rapid rotation limit, the system of governing equations becomes stiff and cannot be handled numerically as such. For this reason, all numerical simulations are, despite the use of state-of-the-art computational resources, performed in a parameter regime far off the relevant values. This stiffness of the equations is directly related to extreme values taken by ratios of typical time scales or typical length scales in the problem. In numerical simulations, however, the controlling parameters assume

† Email address for correspondence: dormy@phys.ens.fr

https://doi.org/10.1017/jfm.2015.747 Published online by Cambridge University Press

much more moderate values, and the corresponding time scales or length scales are necessarily harder to distinguish.

Most numerical models rely on the Boussinesq approximation (incompressible fluid, except inasmuch as the buoyancy force is concerned) and rely on an imposed temperature gradient across the Earth's core to drive thermal convection. Such numerical models, produced to date, appear to fall in two categories. For moderate values of the control parameter, the Rayleigh number, the produced magnetic field is largely dipolar axial, similar in that respect to the Earth's magnetic field. It can exhibit time variations, but does not reverse polarity (Christensen, Olson & Glatzmaier 1999; Kutzner & Christensen 2002). At larger values of the Rayleigh number, a secondary bifurcation occurs, leading to a 'multipolar' and fluctuating dynamo phase (Kutzner & Christensen 2002).

The nature of the dynamo onset (i.e. the bifurcation from the purely hydrodynamic state to the first dynamo mode) has been studied in detail in Morin & Dormy (2009). We reported supercritical, subcritical and isola bifurcation diagrams depending on the values of the parameters. A mechanism for the subcritical bifurcations, in terms of helicity enhancement, has been proposed by Sreenivasan & Jones (2011) (see also Dormy 2011). The transition at larger forcing between the dipolar and multipolar phases has been identified as being controlled by the relative strength of the curl of inertial forces to that of either the viscous or the Coriolis term (see Oruba & Dormy 2014*b*).

These two branches have also been reported in the presence of a uniformly heated fluid as mean dipole (MD) and fluctuating dipole (FD) (Simitev & Busse 2009). The hysteretic nature of this transition and the existence of a domain of bistability has been stressed by many authors (Goudard & Dormy 2008; Simitev & Busse 2009). Schrinner *et al.* (2012) show that, in the presence of stress-free boundary conditions, the same transition occurs, and that the strong hysteresis is associated with the particular nature of geostrophic flows. A similar behaviour is to be expected in the presence of rigid boundary conditions, when viscous effects are small enough.

The present paper focuses on a different mode, characterised by a regime in which both inertia and viscosity are negligible, and the Lorentz force relaxes the constraints imposed by rapid rotation.

2. Governing equations

Thermal convection and magnetic field generation in the Earth's core are modelled in the present study using the most classical set of equations. The rotating incompressible MHD equations are coupled to the heat equation under the Boussinesq approximation. Convection is driven by an imposed temperature difference across a spherical shell (of inner radius r_i and outer radius r_o). Magnetic field generation by dynamo action requires a flow with an appropriate geometry and sufficient amplitude, which can be achieved if the control parameter (measuring the efficiency of the thermal driving) is increased away from the onset of convection. The parameter space for such dynamos has been extensively studied by Christensen and collaborators (e.g. Christensen *et al.* 1999), providing a detailed description of the 'phase diagram' for dynamo action in this set-up (i.e. the region in the parameter space for which different dynamo solutions are produced). The governing equations are solved in a spherical shell ($r_i/r_o = 0.35$) and in a rotating reference frame. The reference frame is such that the velocity vanishes on both spheres (no-slip boundaries), a temperature difference is maintained for all time across the shell, and both the inner and the outer

https://doi.org/10.1017/jfm.2015.747 Published online by Cambridge University Press

domains are assumed electrically insulating. The equations governing the velocity $\boldsymbol{u}$, magnetic field $\boldsymbol{B}$ and temperature field T are then, in non-dimensional form,

$$\frac{E}{Pm}[\partial_t \boldsymbol{u} + (\boldsymbol{u}\cdot\boldsymbol{\nabla})\boldsymbol{u}] = -\boldsymbol{\nabla}\pi + E\Delta\boldsymbol{u} - 2\boldsymbol{e}_z\times\boldsymbol{u} + Ra\,qT\boldsymbol{r} + (\boldsymbol{\nabla}\times\boldsymbol{B})\times\boldsymbol{B}, \quad (2.1)$$

$$\partial_t \boldsymbol{B} = \boldsymbol{\nabla}\times(\boldsymbol{u}\times\boldsymbol{B} - \boldsymbol{\nabla}\times\boldsymbol{B}), \quad \partial_t T + (\boldsymbol{u}\cdot\boldsymbol{\nabla})T = q\Delta T, \quad (2.2a,b)$$

$$\text{with } \boldsymbol{\nabla}\cdot\boldsymbol{u} = \boldsymbol{\nabla}\cdot\boldsymbol{B} = 0. \quad (2.3)$$

In the above equations $L = r_o - r_i$ has been used as length scale, $\tau_\eta = L^2/\eta$ as time scale, and $(\Omega\mu_0\rho_0\eta)^{1/2}$ as magnetic field scale. This non-dimensional form is well suited for strong-field dynamos (e.g. Fearn 1998). The following non-dimensional numbers have been introduced: the Ekman number $E = \nu/\Omega L^2$, the magnetic Prandtl number $Pm = \nu/\eta$, the Roberts number $q = \kappa/\eta$, and the Rayleigh number $Ra = \alpha g\Delta TL/\kappa\Omega$, where $g = g_o/r_o$ with g_o the gravity at $r = r_o$ (note that the Rayleigh number is here modified from its most standard definition to account for the stabilising effect of rotation). It is also useful to define the Prandtl number $Pr = \nu/\kappa \equiv Pm/q$. In the present work, E is set to 3×10^{-4} and Pr to unity; thus it follows that $q = Pm$ in the sequel.

These equations are numerically integrated using the Parody code, originally developed by the author and improved with several collaborators (see Dormy 1997; Schrinner *et al.* 2012). The numerical resolution in the simulations reported here is 132 grid points in radius, with spherical harmonic decomposition of degrees up to $\ell_{max} = 256$ and modes up to $m_{max} = 64$. The models were integrated for up to 10 magnetic diffusion times. In order to ensure the validity of the new solutions presented here, these simulations were also kindly reproduced by V. Morin using the Magic code, developed by Glatzmaier and modified by Christensen and J. Wicht. Both codes have been validated through an international benchmark (see Christensen *et al.* 2001).

3. Weak- and strong-field dynamos

Following the same approach as Morin & Dormy (2009), we study the bifurcation from the purely hydrodynamic solution to the dynamo state using the Rayleigh number as control parameter. At fixed E and Pm, the Rayleigh number needs to exceed a given value for a dynamo solution (non-vanishing field) to exist. We report here direct numerical simulations performed at large values of the magnetic Prandtl number Pm. One may object that such a parameter regime is irrelevant to dynamo action in liquid metals (characterised by a small magnetic Prandtl number). We will however argue that considering large values of Pm can compensate for the excessive role of inertial terms in numerical dynamo models, and is a necessary consequence of the large values assumed by the Ekman number.

Figure 1 presents the bifurcation diagrams obtained for $Pm = q = 14$ and $Pm = q = 18$. The magnetic field strength, as measured by the classical Elsasser number $\Lambda = B^2/(2\Omega\rho\mu\eta)$ is represented versus the Rayleigh number, normalised by its value at the onset of thermal convection Ra_c (here $Ra_c = 60.8$). Each point on this figure corresponds to a time-averaged fully three-dimensional simulation. The time variability of the dynamo mode is reported using the standard deviation.

Figure 1 is characterised by a supercritical bifurcation (as reported in Morin & Dormy (2009) for their 'large' values of the magnetic Prandtl number, i.e. $Pm = 6$).

https://doi.org/10.1017/jfm.2015.747 Published online by Cambridge University Press

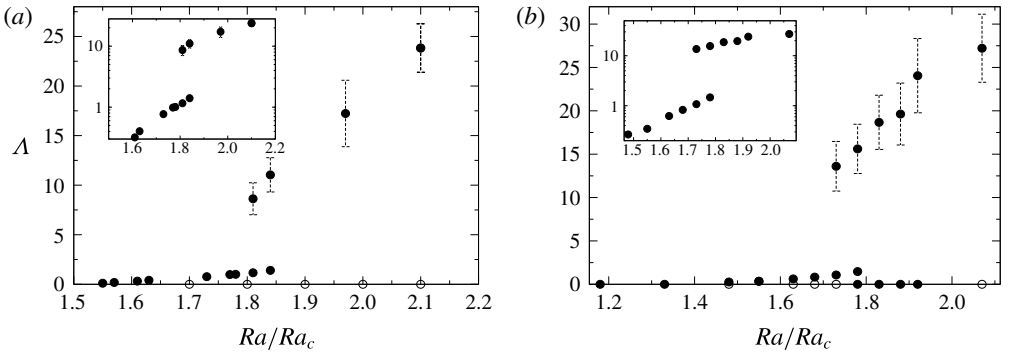


FIGURE 1. Weak- and strong-field branches for $E = 3 \times 10^{-4}$ and for (*a*) $Pm = 14$ and (*b*) $Pm = 18$. Symbols indicate the time-averaged Elsasser number (●, stable; ○, unstable); the time variability of the dynamo mode is reported using the standard deviation (indicated with error bars). The insets present the same graphs in lin–log scale, so that the weak branch is more clearly visible.

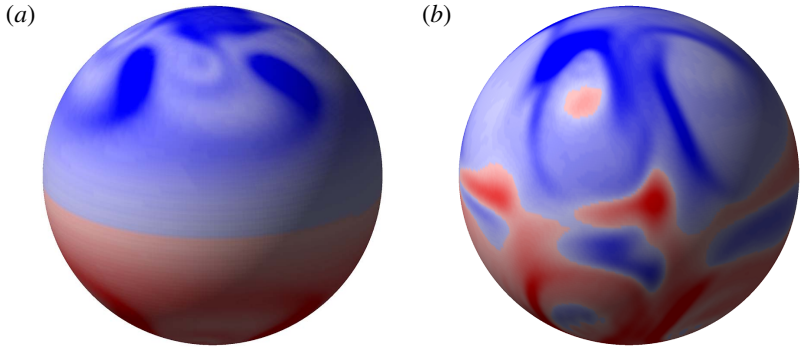


FIGURE 2. (Colour online) Radial component of the magnetic field produced at the surface of the model for $Pm = 18$ and $Ra/Ra_c = 1.73$ on the weak-field (*a*) and strong-field (*b*) branches. The field is characterised by a strong axial dipolar component on both branches.

However, this first dynamo branch rapidly destabilises to a second branch of much stronger amplitude. This strong-field branch can be maintained for decreasing values of the Rayleigh number. The magnetic field is dominated by the axial dipole on both branches (see figure 2). The strong-field branch on figure 1(*a*) is hysteretic to the onset of the dynamo itself: once on this branch, the control parameter can be decreased below the critical value for dynamo bifurcation, while maintaining a dipolar magnetic field.

This new branch completes the sequence of bifurcation diagrams introduced in Morin & Dormy (2009), and the complete three-dimensional bifurcation diagram (including the results of Morin & Dormy (2009)) for $E = 3 \times 10^{-4}$ and $Pr = 1$ is reported on figure 3 versus Ra/Ra_c and Pm. The corresponding two-dimensional bifurcation diagrams, for lower values of Pm, are available in Morin & Dormy (2009).

https://doi.org/10.1017/jfm.2015.747 Published online by Cambridge University Press

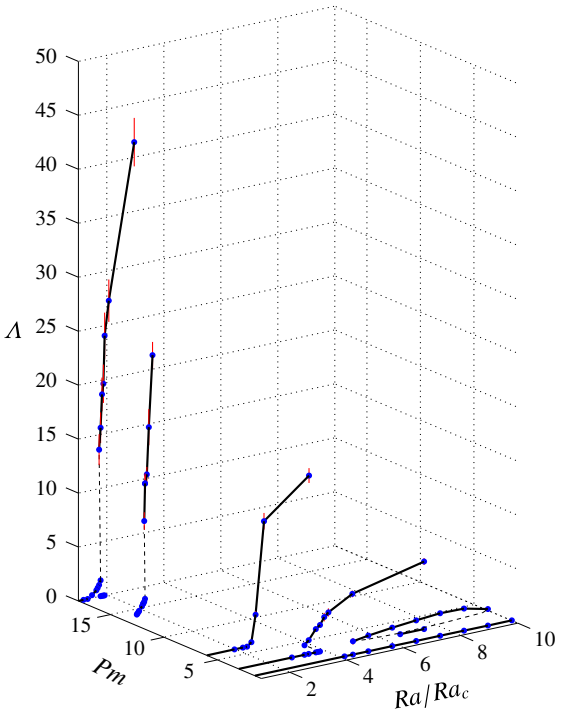


FIGURE 3. (Colour online) Three-dimensional bifurcation diagram for a fixed Ekman number $E = 3 \times 10^{-4}$. Solid lines mark linear interpolation between realised direct numerical simulations. Dashed lines offer a plausible interpretation of the unstable branches.

On such a three-dimensional diagram, the dynamo bifurcation can also be envisaged at fixed value of Ra/Ra_c and varying Pm.

Figure 3 demonstrates how the transition between the different types of bifurcation takes place for different values of Pm. The study of Morin & Dormy (2009) indicates that, as E is decreased (in the moderate range numerically achievable), the overall bifurcation diagram remains largely unaltered but shifted towards lower values of Pm and larger Ra/Ra_c.

Transitions between these two branches of dynamo solutions are obtained by varying only slightly the control parameter at the edge of a given branch. This can produce either a runaway field growth (figure 4*a*), or a catastrophic collapse (figure 4*b*) of the magnetic field. The time at which the forcing (as measured by the Rayleigh number) has been modified (by less than 3 % in each case) is indicated by an arrow on each graph.

No significant changes on the typical length scale of the flow can be reported by comparing the weak- and strong-field branches. This is probably due to the fact that the viscous length scale is not very small at the value of the Ekman number considered here (3×10^{-4}). Smaller values of the Ekman number are undoubtedly needed if one is to appreciate a change in the typical length scale of the flow. One can note however that the Nusselt number is 80 % larger on the strong-field branch than on the weak-field branch.

https://doi.org/10.1017/jfm.2015.747 Published online by Cambridge University Press

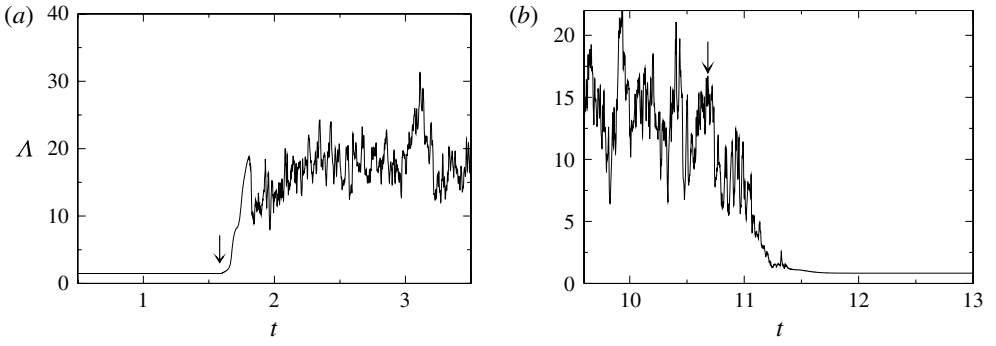


FIGURE 4. Transition between the weak- and strong-field branches for $E = 3 \times 10^{-4}$ and $Pm = 18$ (same as figure 1*b*). Runaway growth from the weak- to the strong-field branch as Ra/Ra_c is increased (arrow) from 1.78 to 1.83 (*a*) and catastrophic decay to the weak-field branch as it is decreased (arrow) from 1.73 to 1.68 (*b*). The lower branch (left part of (*a*) and right part of (*b*) corresponds to small, but non-vanishing, magnetic fields.

4. Force balance

The bifurcation diagram presented on figure 1 is reminiscent of a longstanding theoretical expectation originally introduced as the 'weak'- and 'strong'-field branches (see Roberts 1978; Roberts & Soward 1992). The existence of these two branches in the limit of vanishing viscous forces was introduced through the investigation of magneto-convection studies (for reviews, see Fearn, Roberts & Soward 1986; Proctor 1994).

Soward (1979) investigated the onset of magneto-convection in the cylindrical annulus configuration with sloping boundaries. He found that in most cases the critical Rayleigh number first starts to increase with the Elsasser number, until $\Lambda \sim O(E^{1/3})$, before decreasing. This pointed to the probable existence of a weak-field branch, and the occurrence of a turning point marking the end of the weak-field branch when $\Lambda \sim O(E^{1/3})$. Simultaneously, Fearn (1979*a*,*b*) performed a similar study in the spherical geometry. There again, the Rayleigh number for the thermal Rossby mode may first increase with increasing Elsasser number, yet it eventually decreases to reach a minimum for $\Lambda \sim O(1)$. A more recent study of magneto-convection (Jones *et al.* 2003) focused on the 'weak-field' regime and confirmed its existence.

The above asymptotic scenario assumes a small value of both E and Pm, whereas direct numerical simulations in the self-excited dynamo regime require overestimated values of both numbers.

In order to test the above ideas in the numerical simulations, we need to investigate the dominant force balance relevant to these dynamo modes. Figure 5 presents an instantaneous cross-section of the zonal velocity on both branches for a given parameter set ($Pm = 18$, $Ra/Ra_c = 1.73$). The contour intervals are equally spaced between the minimum and the maximum value for each figure. The zonal flow is nearly three times larger on figure 5(*a*), so that the contour intervals are not identical on the two plots. On the one hand, the weak-field branch saturates while the zonal flow remains essentially geostrophic; the flow is characterised by quasi-geostrophic convection columns. The zonal flow on the strong-field branch, on the other hand, strongly departs from bidimensionality, demonstrating that the rapid rotation constraint has been relaxed. On figure 5(*b*), a localised jet appears near the equator, which marks

https://doi.org/10.1017/jfm.2015.747 Published online by Cambridge University Press

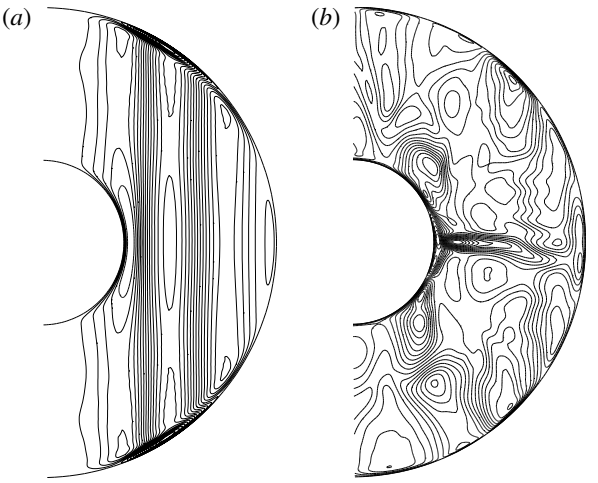


FIGURE 5. Azimuthal velocity in a meridional cross-section for an arbitrary time on the weak-field branch (*a*) and on the strong-field branch (*b*) for the same parameter set ($Pm = 18$, $Ra/Ra_c = 1.73$).

a clear departure from geostrophy. The flow is in general less anisotropic along the direction of the axis of rotation. If this corresponds to the weak-field versus strong-field branches as introduced by Roberts, it implies that the Lorentz forced has achieved a balance with the Coriolis term and thus relaxed the rapid rotation constraint. This dominant balance is usually referred to as the 'magnetostrophic balance'.

The Elsasser number Λ was introduced to measure an order of magnitude of the relative strength of the Lorentz force with respect to the Coriolis force. It achieves this aim remarkably well in asymptotic studies, for the huge distinction between the strong-field balance, characterised by $\Lambda \sim O(1)$, and the weak-field branch, characterised by $\Lambda \sim O(E^{1/3})$. In numerical works, however, as small parameters (such as the Ekman number) are not asymptotically small, the measure provided by this non-dimensional number is then not accurate enough. Finer estimates of this force balance can then be constructed. Introducing $\{\cdot\}$ as an 'order-of-magnitude' operator, we can write

$$\frac{\{(\mu\rho)^{-1}\boldsymbol{\nabla}\times\boldsymbol{B}\times\boldsymbol{B}\}}{\{2\Omega\times\boldsymbol{u}\}} = \frac{B^2}{2\Omega\mu\rho U\ell_B}, \tag{4.1}$$

where U is a typical, say root mean square (r.m.s.), value for the velocity field, B a typical value for the magnetic field, and ℓ_B the typical magnetic dissipation length scale (see also Oruba & Dormy 2014*a*).

The classical definition of the Elsasser number is obtained by assuming $\ell_B \sim L$ and a statistical balance between induction and diffusion of the magnetic field,

$$\{\boldsymbol{\nabla}\times(\boldsymbol{u}\times\boldsymbol{B})\} \sim \{\eta\boldsymbol{\nabla}\times\boldsymbol{\nabla}\times\boldsymbol{B}\}, \tag{4.2}$$

which yields $U \sim \eta/L$. Then (4.1) provides the standard expression for the Elsasser number $\Lambda = B^2/(2\Omega\rho\mu\eta)$. This expression provides a sensible description of the force balance for asymptotic studies, yet finer estimates appear to be needed for numerical studies.

https://doi.org/10.1017/jfm.2015.747 Published online by Cambridge University Press

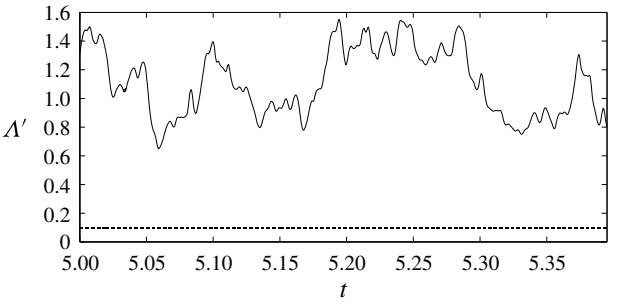


FIGURE 6. Fluctuation of the modified Elsasser number on both branches for the same parameter set ($Pm = 18$, $Ra/Ra_c = 1.73$).

Branch	Ra	Ra/Ra_c	Pm	Rm	ℓ_B	Λ	Λ'
Weak	105	1.73	18	195	0.097	1.14	0.06
Strong	105	1.73	18	145	0.082	13.6	1.14
Strong	125	2.05	18	207	0.075	27.2	1.75
Strong	112	1.84	14	150	0.083	11.05	0.89

TABLE 1. Typical estimates of the Elsasser number and the modified Elsasser number ($\Lambda' = \Lambda L/(Rm\ell_B)$, see text) on the weak- and strong-field branches. The modified Elsasser number offers a finer measurement of the force balance.

One can note, for example, that $U \sim \eta/L$ amounts to assuming $Rm \sim O(1)$. A finer description of the force balance (4.1) can be obtained by estimating U via $Rm\,\eta/L$. Inserting this definition in (4.1) yields

$$\Lambda' = \frac{B^2 L}{2\Omega\rho\mu\eta Rm\,\ell_B} = \Lambda\frac{L}{Rm\,\ell_B}. \tag{4.3}$$

Table 1 presents a comparison of the classical Elsasser number Λ and the modified Elsasser number Λ' on both branches. The magnetic Reynolds number Rm is here defined on the r.m.s. velocity, and the typical magnetic dissipation length scale ℓ_B is defined, as in Oruba & Dormy (2014*a*), as

$$\ell_B^2 = \frac{\displaystyle\int_V \boldsymbol{B}^2\,\mathrm{d}V}{\displaystyle\int_V (\boldsymbol{\nabla}\times\boldsymbol{B})^2\,\mathrm{d}V}. \tag{4.4}$$

Figure 6 presents the time variation of the modified Elsasser number on the weak-field branch (dashed) and on the strong-field branch (solid line) for the same parameter set, $Pm = 18$, $Ra/Ra_c = 1.73$.

The modified Elsasser number, offering a finer description of the force balance, reveals that the Lorentz force is significantly weaker than the Coriolis force on the weak-field branch and that the two terms are indeed of comparable amplitude on the strong-field branch.

The orders of magnitude derived above indicate that the anticipated balance between the Coriolis and Lorentz forces is plausible. To achieve a finer validation than simple

https://doi.org/10.1017/jfm.2015.747 Published online by Cambridge University Press

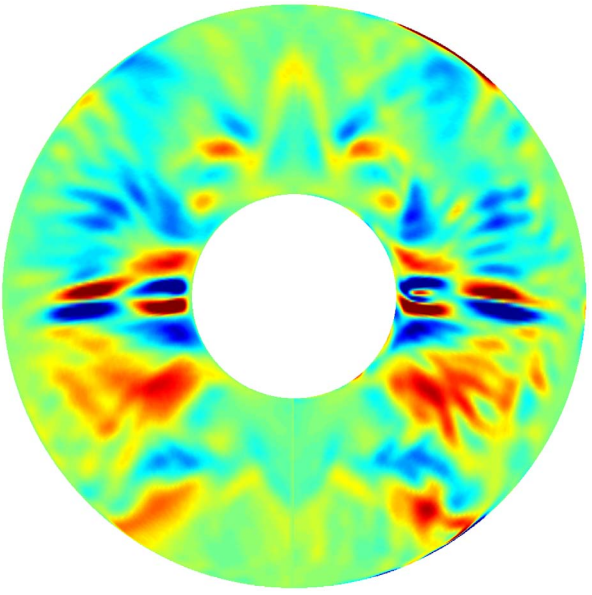


FIGURE 7. (Colour online) Meridional cross-sections on the strong-field branch at a given time for the same parameters and same phase as in figure 5(*b*). On the left side is presented $-2\partial \boldsymbol{u}/\partial z \cdot \boldsymbol{e}_r$, and on the right side $(\boldsymbol{\nabla} \times ((\boldsymbol{\nabla} \times \boldsymbol{B}) \times \boldsymbol{B})) \cdot \boldsymbol{e}_r$ using the same colour range.

orders of magnitude, we can assess whether the two terms tend to balance each other locally in space. To this aim, one can consider the curl of the momentum equation (2.1), neglecting both the inertial term and the viscous term,

$$-2\frac{\partial \boldsymbol{u}}{\partial z} \sim Ra\, q \boldsymbol{\nabla} \times (T\boldsymbol{r}) + \boldsymbol{\nabla} \times ((\boldsymbol{\nabla} \times \boldsymbol{B}) \times \boldsymbol{B}). \tag{4.5}$$

If we now consider the radial component of the above equation, i.e. its toroidal component, the first term on the right-hand side disappears. The remaining two terms were computed numerically at a given instant in time and on a cross-section in an arbitrary meridional plane. These quantities are presented on figure 7.

Deviations between the two cross-sections can imply only non-vanishing inertial and/or viscous effects. Estimations of these terms reveals that the viscous term accounts for the differences visible on the figures (inertia being one order of magnitude smaller). The comparison reveals such effects (in particular, in viscous boundary layers), but otherwise clearly demonstrates that the radial component of the curl of the Lorentz force balances that of the Coriolis force, as expected in the strong-field limit.

The viscous force will of course not always be negligible in the parameter regime considered here. It can be more important at some places or times. To illustrate this, the quantities represented on figure 7 are represented at a later time in the form of three-dimensional isosurfaces on figure 8. The blue and red isosurfaces, respectively, correspond to $\pm 90\,\%$ of the peak values. While deviations from magnetostrophy are obvious, in particular comparing the centre of each figure, the dominant magnetostrophic balance is highlighted. Deviations are here primarily due to viscous forces. Boundary layers have not been represented in these figures.

https://doi.org/10.1017/jfm.2015.747 Published online by Cambridge University Press

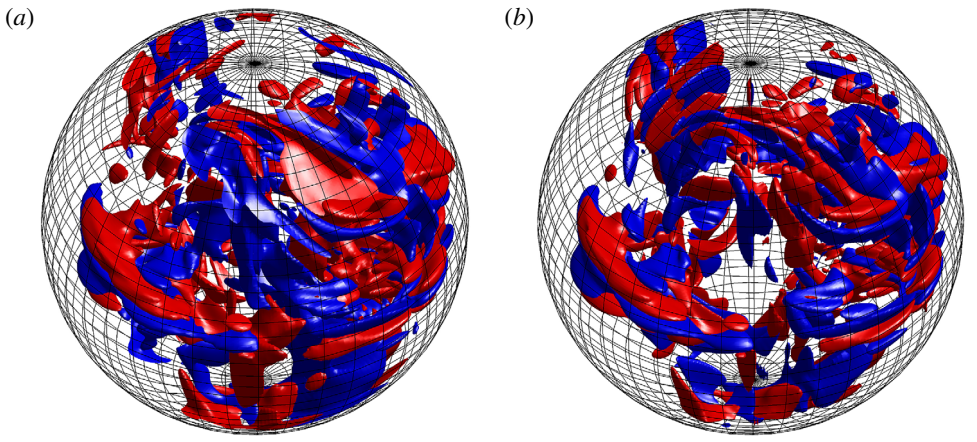


FIGURE 8. (Colour online) Three-dimensional isosurfaces of the radial component of the curl of the Coriolis force (*a*) and the Lorentz force (*b*).

Figures 7 and 8 highlight the balance between the non-gradient part of the Lorentz and Coriolis terms. Differences are primarily due to viscous effects and remain small (but non-vanishing) on average. The r.m.s. value of the sum of the two quantities plotted in these figures, averaged in time, exceeds by a factor 5 that of their difference.

5. Discussion

Numerical models of self-excited dynamos usually correspond to two distinct branches, either viscous–dipolar or inertial–multipolar (e.g. Kutzner & Christensen 2002; Jones 2011; Oruba & Dormy 2014*b*). This work introduces a third dynamo branch in the parameter regime that is numerically achievable with present computational resources. What if this new branch was relevant to the geodynamo?

5.1. *Physical interpretation*

In numerical models, at moderate Ekman numbers, inertial forces increase too rapidly with the control parameter (the Rayleigh number) to allow for a strong-field branch balance (the magnetic field amplitude does not increase rapidly enough, and inertial forces enter the dominant balance before the Lorentz force). In order to observe at a given Ekman number the third branch introduced in this work, one needs to increase the magnetic Prandtl number in order to decrease the prefactor of inertial forces. This results in a larger magnetic Reynolds number for a given value of the Rayleigh number.

Using large values of the magnetic Prandtl number thus allows for the runaway field solution anticipated theoretically. We observe that the Lorentz force becomes large enough (while inertia remains small enough not to modify the nature of dynamo action) in order for the Lorentz force to relax the constraints of rapid rotation.

The three-dimensional bifurcation diagram (figure 3) can be tentatively sketched near the region in which the strong- and weak-field branches coexist (see figure 9). The change of branch as Ra is varied at fixed Pm corresponds to a fold of the surface of solutions. It is clear from such a representation that, in the two-dimensional parameter space (E, Pm), one can continuously move from the lower to the upper

https://doi.org/10.1017/jfm.2015.747 Published online by Cambridge University Press

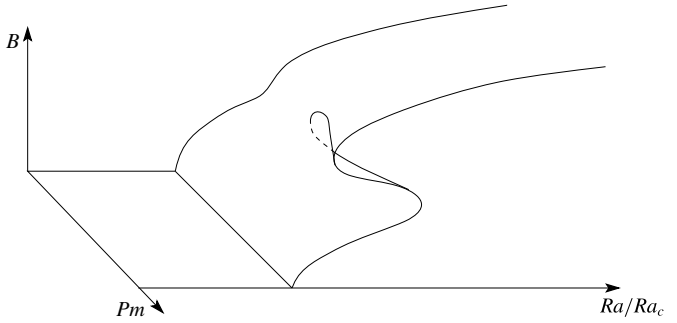


FIGURE 9. Sketch of a tentative two-dimensional bifurcation diagram near the region of existence of the weak- and strong-field branches. The fold in the surface accounts for the observed two branches of solutions.

branch, avoiding the fold singularity. The corresponding intermediate models would presumably involve a continuous decrease of viscous forces. These intermediate solutions (at lower values of Pm) will then have characteristics continuously varying from that of the weak branch to that of the strong branch. It follows that some numerical models obtained at lower values of Pm will necessarily have some characteristics of the strong-field branch. Such is the case in particular for models with a large magnetic Prandtl number (though not large enough for the bistability to occur) and large Rayleigh number (so that viscous effects are reduced), but not too large (to avoid the inertial, non-dipolar, branch). In such a model, time-averaged force balance can tend to magnetostrophy (e.g. Aubert 2005; Sreenivasan, Sahoo & Jones 2014).

It should be stressed as well that large values of Pm have been studied in a few earlier numerical works (e.g. Gubbins *et al.* 2007; Olson *et al.* 2011), though without pointing to the existence of a weak- and a strong-field branch.

5.2. *Distinguished limit*

We have seen in Morin & Dormy (2009) that the nature of the dynamo bifurcation strongly depends on the parameters (in particular, Pm at fixed E). The current approach to geodynamo modelling consists either in trying to explore the whole range of magnetic Prandtl number at fixed Ekman number, or, too often, in trying to decrease the value of the magnetic Prandtl number as low as possible for a given Ekman number (the viscous dipolar solution being lost for Pm lower than a critical value Pm_c). The present work suggests that, in order to preserve the relevant force balance, both E and Pm being small parameters in the Earth's core, they could be related in numerical studies via a distinguished limit, involving only one small parameter ε. Ideally, the nature of the dynamo bifurcation should be preserved in the limiting process.

In order to propose such a scaling, one could be guided by the scaling for the minimum magnetic Prandtl number Pm_c as a function of the Ekman number E. This relations stems from numerical simulations in the viscous branch; it is however the only regime that has been widely covered in numerical simulations. The available data are illustrated in figure 10. Decreasing Pm at otherwise fixed parameters amounts to decreasing the magnetic Reynolds number. The dipolar viscous branch is thus lost for $Pm < Pm_c$, which decreases with decreasing values of the Ekman number (Kutzner

https://doi.org/10.1017/jfm.2015.747 Published online by Cambridge University Press

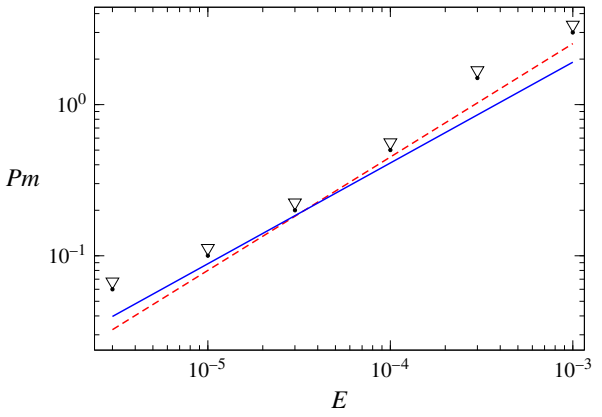


FIGURE 10. (Colour online) Minimal value of the magnetic Prandtl number Pm_c below which the dipolar viscous branch is lost for a given Ekman number. Triangles correspond to numerical data produced by Christensen & Aubert (2006), and the dashed line to their empirical fit $Pm_c \sim E^{3/4}$. The solid line corresponds to the $Pm_c \sim E^{2/3}$ scaling (Dormy & Le Mouël 2010).

& Christensen 2002; Christensen & Aubert 2006). It follows a scaling of the form $Pm_c \sim E^{\alpha}$, in which α needs to be determined. Christensen & Aubert (2006) proposed an empirical fit with $\alpha = 3/4$. Dormy & Le Mouël (2010) proposed, on the basis of exponential growth associated with a locally time-dependent shear, a scaling of the form $\alpha = 2/3$, which seems to match the numerical data equally well and is guided by a plausible argument. For simplicity, we will use this latter scaling for illustration purposes below, but the same reasoning would apply with a different exponent.

In order to introduce a single small parameter ε to control both quantities, one can write $E \sim A\varepsilon^B$ and $Pm \sim C\varepsilon^D$. Without loss of generality, one can set $A = 1$, up to a redefinition of ε. In order to preserve the nature of the dynamo bifurcation in the limiting process, we propose $Pm^3 \sim E^2$, and it follows that

$$E \sim \varepsilon^3, \quad Pm \sim C\varepsilon^2. \tag{5.1a,b}$$

This distinguished limit ensures that both E and Pm tend to zero with ε and that they are related in such a way that the nature of the solution, i.e. its dynamo property, should be preserved in the limiting process. The coefficient C can be estimated via sensible estimates for the Earth's core, such as $E \simeq 10^{-14}$ and $Pm \simeq 10^{-6}$: the first equation naturally provides $\varepsilon \simeq 2 \times 10^{-5}$, while the second yields $C \simeq 2 \times 10^3$, which is a rather large prefactor. Applying (5.1) to the numerical models presented in this work (with $E = 3 \times 10^{-4}$), in turn yields $Pm \simeq 10$. This distinguished limit thus yields values of the magnetic Prandtl number larger than unity (similar to those used in our numerical studies) for the Ekman number investigated here.

The idea behind such distinguished limits is not to aim at a large magnetic Prandtl number limit, as both the Ekman number and the Prandtl number vanish asymptotically in the limiting process. For the moderate values of the small parameter ε, achievable with current computational resources, the proposed distinguished limit however suggests that the use of values of Pm larger than unity is relevant.

As computational resources increase, one should be able in the near future to investigate the behaviour of this strong-field branch for lower values of the Ekman

https://doi.org/10.1017/jfm.2015.747 Published online by Cambridge University Press

number, and thus lower values of the magnetic Prandtl number. This will allow investigation of interesting and important issues, in particular on the evolution of the relevant length scale as the magnetic Prandtl number becomes less than unity.

6. Conclusions

A dominant magnetostrophic balance can be established in direct numerical simulations of rotating spherical dynamos. Magnetostrophy is not satisfied everywhere and for all time.

The weak- and strong-field branches anticipated from asymptotic studies of magneto-convection are approached in direct numerical simulations for some parameter values. In order for inertial forces to be small enough to allow this regime, it is necessary to relate the magnetic Prandtl number to the Ekman number in the form of a distinguished limit. Further studies will need to decrease the Ekman number to ensure a clear distinction between the small-scale flow on the viscous branch and the large-scale flow on the strong-field branch. The next important challenge for direct numerical models would be to maintain dynamo action for $Ra/Ra_c < 1$ as expected theoretically. The role of the Prandtl number (fixed to unity here) in controlling the relative strength of the advection versus diffusion of heat also deserves further studies. Further numerical studies of this branch could include varying Pr. For instance the limit of large Pm with small q would allow for significant nonlinearities in the energy equation, while controlling the amplitude of inertial effects.

Acknowledgements

The author is very grateful to V. Morin, L. Petitdemange and L. Oruba for their help at various stages of the preparation of this article. S. Fauve provided useful comments on earlier versions of this work. Computations were performed on the CEMAG parallel computer and on the HPC resources of MesoPSL, financed by the Region Ile de France and the project Equip@Meso (reference ANR-10-EQPX-29-01) of the programme Investissements d'Avenir supervised by the Agence Nationale pour la Recherche.

REFERENCES

AUBERT, J. 2005 Steady zonal flows in spherical shell dynamos. *J. Fluid Mech.* **542**, 53–67.

CHRISTENSEN, U. & AUBERT, J. 2006 Scaling properties of convection-driven dynamos in rotating spherical shells and application to planetary magnetic fields. *Geophys. J. Intl* **166**, 1–97.

CHRISTENSEN, U., AUBERT, J., CARDIN, P., DORMY, E., GIBBONS, S., GLATZMAIER, G., HONKURA, Y., JONES, C., KONO, M. *et al.* 2001 A numerical dynamo benchmark. *Phys. Earth Planet. Inter.* **128**, 25–34.

CHRISTENSEN, U., OLSON, P. & GLATZMAIER, G. 1999 Numerical modelling of the geodynamo: a systematic parameter study. *Geophys. J. Intl* **138**, 393–409.

DORMY, E. 1997 Modélisation numérique de la dynamo terrestre. PhD thesis, IPGP.

DORMY, E. & SOWARD, A. M. (Eds) 2007 *Mathematical Aspects of Natural Dynamos*. CRC.

DORMY, E. & LE MOUËL, J.-L. 2008 Geomagnetism and the dynamo: where do we stand? *C. R. Acad. Sci. Paris* **9**, 711–720.

DORMY, E. 2011 Stability and bifurcation of planetary dynamo models. *J. Fluid Mech.* **688**, 1–4.

FEARN, D. R. 1979*a* Thermally driven hydromagnetic convection in a rapidly rotating sphere. *Proc. R. Soc. Lond.* A **369** (1737), 227–242.

FEARN, D. R. 1979*b* Thermal and magnetic instabilities in a rapidly rotating fluid sphere. *Geophys. Astrophys. Fluid Dyn.* **14** (1), 103–126.

https://doi.org/10.1017/jfm.2015.747 Published online by Cambridge University Press

FEARN, D. R. 1998 Hydromagnetic flow in planetary cores. *Rep. Prog. Phys.* **61**, 175–235.

FEARN, D. R., ROBERTS, P. H. & SOWARD, A. M. 1986 Convection, stability and the dynamo. In *Energy Stability and Convection* (ed. G. P. Galdi & B. Straughan), Proceedings of the Workshop, Capri, Longman Scientific & Technical.

GOUDARD, L. & DORMY, E. 2008 Relations between the dynamo region geometry and the magnetic behavior of stars and planets. *Europhys. Lett.* **83**, 59001.

GUBBINS, D., WILLIS, A. & SREENIVASAN, B. 2007 Correlation of Earth's magnetic field with lower mantle thermal and seismic structure. *Phys. Earth Planet. Inter.* **162**, 256–260.

JONES, C. A. 2011 Planetary magnetic fields and fluid dynamos. *Annu. Rev. Fluid Mech.* **43**, 583–614.

JONES, C. A., MUSSA, A. I. & WORLAND, S. J. 2003 Magnetoconvection in a rapidly rotating sphere: the weak-field case. *Proc. R. Soc. Lond.* A **459**, 773–797.

KUTZNER, C. & CHRISTENSEN, U. 2002 From stable dipolar towards reversing numerical dynamos. *Phys. Earth Planet. Inter.* **131**, 29–45.

MOFFATT, H. K. 1978 *Magnetic Field Generation in Electrically Conducting Fluids*. Cambridge University Press.

MORIN, D. & DORMY, E. 2009 The dynamo bifurcation in rotating spherical shells. *Intl J. Mod. Phys.* B **23**, 5467–5482.

OLSON, P., GLATZMAIER, G. & COE, R. 2011 Complex polarity reversals in a geodynamo model. *Earth Planet. Sci. Lett.* **304**, 168–179.

ORUBA, L. & DORMY, E. 2014*a* Predictive scaling laws for spherical rotating dynamos. *Geophys. J. Intl* **198**, 828–847.

ORUBA, L. & DORMY, E. 2014*b* Transition between viscous dipolar and inertial multipolar dynamos. *Geophys. Res. Lett.* **41** (20), 7115–7120.

PROCTOR, M. R. E. 1994 Convection and magnetoconvection. In *Lectures on Solar and Planetary Dynamos* (ed. M. R. E. Proctor & A. D. Gilberts). Cambridge University Press.

ROBERTS, P. H. 1978 Magneto-convection in a rapidly rotating fluid. In *Rotating Fluids in Geophysics* (ed. P. H. Roberts & A. M. Soward). Academic.

ROBERTS, P. H. 1988 Future of geodynamo theory. *Geophys. Astrophys. Fluid Dyn.* **44**, 3–31.

ROBERTS, P. H. & SOWARD, A. M. 1992 Dynamo theory. *Annu. Rev. Fluid Mech.* **24**, 459–512.

SCHRINNER, M., PETITDEMANGE, L., DORMY, E. & SCHRINNER, M. 2012 Dipole collapse and dynamo waves in global direct numerical simulations. *Astrophys. J.* **752**, 121.

SIMITEV, R. & BUSSE, F. 2009 Bistability and hysteresis of dipolar dynamos generated by turbulent convection in rotating spherical shells. *Eur. Phys. Lett.* **85**, 19001.

SOWARD, A. M. S. 1979 Convection driven dynamos. *Phys. Earth Planet. Inter.* **20**, 134–151.

SREENIVASAN, B. & JONES, C. A. 2011 Helicity generation and subcritical behaviour in rapidly rotating dynamos. *J. Fluid Mech.* **688**, 5–30.

SREENIVASAN, B., SAHOO, S. & JONES, C. A. 2014 The role of buoyancy in polarity reversals of the geodynamo. *Geophys. J. Intl* **199**, 1698–1708.

https://doi.org/10.1017/jfm.2015.747 Published online by Cambridge University Press